APL Materials

Enhanced T_c in SrRuO$_3$/DyScO$_3$(110) thin films with high residual resistivity ratio ⓕ

Nathaniel J. Schreiber ⓘ ; Ludi Miao ⓘ ; Hari P. Nair ⓘ ; Jacob P. Ruf ⓘ ; Lopa Bhatt; Yorick A. Birkholzer ⓘ ; George N. Kotsonis ⓘ ; Lena F. Kourkoutis ⓘ ; Kyle M. Shen ⓘ ; Darrell G. Schlom ✉ ⓘ

Check for updates

View Online

Export Citation

CrossMark

AIP Publishing

Enhanced T_C in SrRuO₃/DyScO₃(110) thin films with high residual resistivity ratio Ⓕ

View Online   Export Citation   CrossMark

Nathaniel J. Schreiber,[1] ⒾⒹ Ludi Miao,[2] ⒾⒹ Hari P. Nair,[1] ⒾⒹ Jacob P. Ruf,[2,3] ⒾⒹ Lopa Bhatt,[4]
Yorick A. Birkholzer,[1] ⒾⒹ George N. Kotsonis,[1] ⒾⒹ Lena F. Kourkoutis,[4,5] Kyle M. Shen,[2,5] ⒾⒹ
and Darrell G. Schlom[1,5,6,a] ⒾⒹ

AFFILIATIONS

[1] Department of Materials Science and Engineering, Cornell University, Ithaca, New York 14853, USA
[2] Department of Physics, Laboratory of Atomic and Solid State Physics, Cornell University, Ithaca, New York 14853, USA
[3] Max-Planck-Institute for Chemical Physics of Solids, Nöthnitzer Str. 40, 01187 Dresden, Germany
[4] School of Applied and Engineering Physics, Cornell University, Ithaca, New York 14853, USA
[5] Kavli Institute at Cornell for Nanoscale Science, Ithaca, New York 14853, USA
[6] Leibniz-Institut für Kristallzüchtung, Max-Born-Str. 2, 12489 Berlin, Germany

[a] Author to whom correspondence should be addressed: schlom@cornell.edu

ABSTRACT

Epitaxial untwinned SrRuO₃ thin films were grown on (110)-oriented DyScO₃ substrates by molecular-beam epitaxy. We report an exceptional sample with a residual resistivity ratio (RRR), ρ [300 K]/ρ [4 K] of 205 and a ferromagnetic Curie temperature, T_C, of 168.3 K. We compare the properties of this sample to other SrRuO₃ films grown on DyScO₃(110) with RRRs ranging from 8.8 to 205, and also compare it to the best reported bulk single crystal of SrRuO₃. We determine that SrRuO₃ thin films grown on DyScO₃(110) have an enhanced T_C as long as the RRR of the thin film is above a minimum electrical quality threshold. This RRR threshold is about 20 for SrRuO₃. Films with lower RRR exhibit T_Cs that are significantly depressed from the intrinsic strain-enhanced value.

I. INTRODUCTION

The Sr$_{n+1}$Ru$_n$O$_{3n+1}$ Ruddlesden–Popper (RP) series, and more broadly the ruthenate family, exhibit wide-ranging phenomena, including superconductivity,[1,2] ferromagnetism,[3] metal-to-insulator transitions,[4] and the spin Hall effect.[5] Nevertheless, the properties of ruthenates are very sensitive to disorder, meaning that in order to understand the intrinsic ground state of ruthenate materials, it is necessary to synthesize samples with exceptionally low disorder. For example, the superconductivity in Sr₂RuO₄ can be destroyed with aluminum impurity concentrations of only 300–450 ppm.[6]

SrRuO₃ is a ferromagnetic metal with a Curie temperature (T_C) of ~160 K[3] in bulk single crystals (reported as high as 163.5 K).[7] The highest reported residual resistivity ratio (RRR) value, ρ [300 K]/ρ [4 K], for a SrRuO₃ single crystal is 162.[7] In order to utilize SrRuO₃ in devices and heterostructures, it must be grown as a thin film. The

quality of thin films lags behind that of bulk samples, with the current record RRR for a SrRuO₃ film being about 80.[8] This record RRR is for a film grown by reactive evaporation. SrRuO₃ films grown by molecular-beam epitaxy (MBE) have RRRs as high as 76,[9–11] whereas the highest RRR reported for films grown by pulsed-laser deposition (PLD) is 14[12] and for sputtering is about 7.[13]

Several studies have highlighted the detrimental effect of ruthenium vacancies in SrRuO₃ samples on the resulting properties.[14] For example, Dabrowski et al. showed that systematically adding ruthenium vacancies significantly reduced T_C from 163 to 45 K.[15] Another study demonstrated that a nonrandom distribution of ruthenium vacancies in SrRuO₃ can lead to anomalous features in the Hall effect measurement that resemble the topological Hall effect signature.[16] Ruthenium vacancies appear to have a significant effect on the magnetic properties of SrRuO₃. Therefore, it is important to synthesize films with minimal defects and disorder to isolate the

intrinsic effects of strain on the properties of $SrRuO_3$ in thin films when compared with bulk samples. The subject of this study is the requisite quality necessary for the measurement of the intrinsic magnetic properties of $SrRuO_3$ thin films.

There have been successful efforts to utilize machine learning to improve film quality, such as by Wakabayashi *et al.*,[11,17,18] leading to the report of a record-breaking T_C of 169 K in one of their $SrRuO_3/DyScO_3(110)$ thin films.[18] Nevertheless, the RRR still remains low compared to bulk samples. Recently, it has become possible to consistently grow high quality $SrRuO_3$ thin films guided by a thermodynamics of molecular-beam epitaxy (TOMBE) diagram.[9] In this work, we report on the growth of a $SrRuO_3/DyScO_3(110)$ thin film by MBE with the highest RRR to date for either a bulk single crystal or a thin film. We confirm the result from Wakabayashi *et al.*, which showed that films grown on $DyScO_3(110)$ actually have an enhanced T_C,[18] by comparing our best films with the bulk T_C. Moreover, we attempt to determine a minimum viable electrical quality, i.e., minimum RRR, needed to accurately conclude the intrinsic effect of strain on the T_C of commensurately strained $SrRuO_3/DyScO_3(110)$. In doing so, we reveal how disorder can easily obscure the intrinsic effect of strain on the T_C of $SrRuO_3$.

II. METHODS

Thin films of $SrRuO_3$ were grown on (110) $DyScO_3$ substrates by oxide MBE in a Veeco Gen10 MBE system. Absorption-controlled growth was optimized utilizing the previously published TOMBE diagram.[9] Films were grown at substrate temperatures in a range of 650–705 °C and at a chamber background pressure of 10^{-6} Torr in a distilled ozone environment (~80% O_3 + 20% O_2). The substrate temperature was measured by using an optical pyrometer operating at a wavelength of 1550 nm. The strontium (99.99%) source material was evaporated from a low-temperature effusion cell, and an electron beam evaporator was used to deposit the ruthenium source material (99.99%). The ratio of strontium to ruthenium (Sr/Ru) in the flux incident on the substrate during growth was varied for the samples presented in this paper and ranged from 1.36 to 3.03. Note that due to the adsorption-controlled growth mode, the excess ruthenium provided is desorbed during growth to produce phase-pure $SrRuO_3$ films. The film growth rate ranged from 3.8 to 6.0 Å/min.

The electrical resistivity of the $SrRuO_3$ samples was measured by wire bonding directly to the sample surface in a 4-point van der Pauw geometry. For comparison, all RRR results shown are for the current flowing along the $[1\bar{1}0]$ direction. The hall bars of the two samples with the highest RRR (Sample G and Sample F) were fabricated with 20×50 μm^2 channels defined by photolithography. The Hall bar channels were formed by argon ion milling, and platinum/titanium pads were subsequently sputtered onto the thin films to form Ohmic contact pads.

The electrical resistivity measurements were performed in a Quantum Design Physical Property Measurement System (PPMS). The samples were cooled from 300 to 4 K, and the resistance was measured during cooling. The best sample was also cooled in another PPMS with He-3 capability to a base temperature of 0.45 K while the resistance was measured. The Hall effect was also measured on the best sample at a temperature of 100 K with the

magnetic field aligned along the magnetic easy axis (~50° away from the surface normal vector). The magnetic field was swept from −4 to 4 T.

X-ray diffraction (XRD) $\theta - 2\theta$ scans and rocking curves (ω) were measured with Cu-Kα_1 radiation using a Rigaku SmartLab high-resolution diffractometer. Reciprocal space maps were collected using a PANalytical Empyrean x-ray diffractometer equipped with a 1/4° divergence slit, a 4 mm beam mask, hybrid 2-bounce channel-cut Ge monochromator incident optics, a dual-axis electronic tilt stage, and a PIXcel3D area detector. Atomic force microscopy (AFM) images were taken with an Asylum Cypher ES Environmental AFM. *In situ* reflection high-energy electron diffraction (RHEED) was monitored to observe surface quality and surface structure during growth.

Cross-sectional scanning transmission electron microscopy (STEM) specimens were prepared by standard focused ion beam (FIB) lift-out with a Thermo Fisher Scientific Helios G4 UX FIB. High-angle annular dark-field scanning transmission electron microscopy (HAADF-STEM) images were acquired on an aberration-corrected FEI Titan Themis 300 operating at 300 kV with a 30 mrad probe convergence semi-angle and an inner (outer) collection angle of 68 (340) mrad.

III. RESULTS AND DISCUSSION

In the resistivity measurements, one $SrRuO_3/DyScO_3(110)$ sample showed exceptional electrical quality, exhibiting a RRR of 205, which represents a new record for $SrRuO_3$ in both thin films and bulk single crystals. In this paper, we are defining RRR as the resistivity at 300 K divided by the resistivity at 4 K (ρ [300 K]/ρ [4 K]). Some papers define RRR in a way that yields higher values than our simple definition by extrapolating the low-temperature resistivity to 0 K before taking the resistivity ratio.[11,19] For such a definition, our film has a RRR of 263. The resistivity as a function of temperature for this film (called the "high-RRR sample" for the rest of the paper) is shown in Fig. 1(a). The resistivity data shown are from a patterned Hall bar to provide a more accurate result than initial measurements made using the van der Pauw method,[20] (which indicated a RRR (ρ [300 K]/ρ [4 K]) of about 250). The inset to Fig. 1(a) shows that the high-RRR sample is metallic down to 0.45 K, the limit of our He-3 PPMS capability. The resistivity at 0.45 K is 1.12 $\mu\Omega$ cm. In $SrRuO_3$, the kink in the resistivity vs temperature plot corresponds to T_C. To highlight the kink in Fig. 1(b), the derivative of the resistivity with respect to temperature is plotted as a function of temperature. The edge of the peak, as shown in Fig. 1(b), corresponds to the kink in Fig. 1(a) and is generally accepted as T_C. Therefore, for the high-RRR sample, T_C is 168.3 K.

To the best of our knowledge, the previous record RRR (ρ [300 K]/ρ [4 K]) for a $SrRuO_3/DyScO_3(110)$ thin film is 74,[21] and for any $SrRuO_3$ thin film, it is about 80.[8] For a bulk single crystal, the record RRR (ρ [300 K]/ρ [4 K]) is 162.[7] (When the low-temperature resistivity is extrapolated to 0 K, the RRR is 192.[7]) Therefore, with a RRR of 205, the high-RRR sample in this paper represents a significant improvement in the electrical quality of $SrRuO_3$ thin films. It is also noteworthy that in this high-RRR sample, the Hall measurement (Fig. S1) shows no resistive anomalies that are reminiscent of the topological Hall effect, consistent with the results shown in Ref. 16.
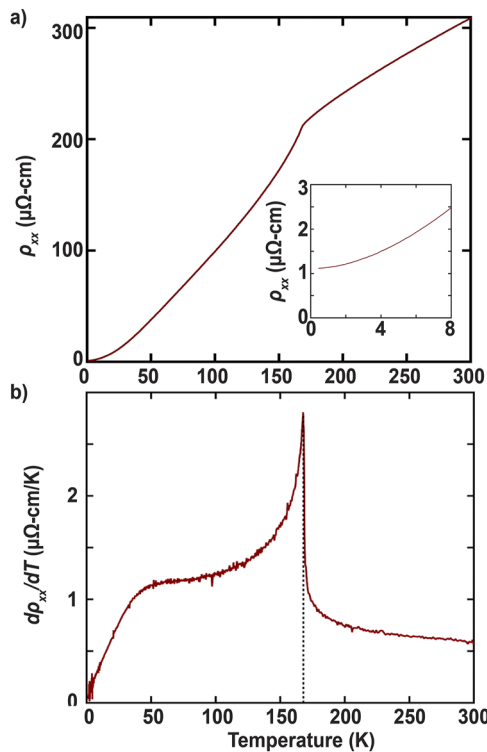
FIG. 1. Electrical resistivity of the high-RRR SrRuO$_3$/DyScO$_3$(110) thin film (RRR = 205). (a) Resistivity as a function of temperature measured as the sample is cooled from 300 to 0.45 K with current flowing along the $\left[1\bar{1}0\right]$ direction. The residual resistivity ratio (RRR), defined in this paper as ρ [300 K]/ρ [4 K], is 205, and the inset figure shows that at 0.45 K, the resistivity is 1.12 $\mu\Omega$ cm. (b) Shown is the derivative of the resistivity with respect to temperature. The dashed line is at T = 168.3 K, which represents the ferromagnetic Curie temperature (T_C) for this sample.

We characterize the structural quality of the high-RRR sample with x-ray diffraction. The lack of spurious peaks in the $\theta - 2\theta$ scan, shown in Fig. S2, indicates that the film is phase pure. Figure 2(a) shows a zoomed-in region around the 220 orthorhombic peak of SrRuO$_3$ with clear Laue fringes, indicating good crystalline quality and a film thickness of 49.8 ± 1 nm. To find the thickness, we use a dynamical x-ray diffraction simulation[22] of the region around the 220 peak. The simulation is plotted on top of the measured 220 peak and shown in Fig. S3. A Nelson–Riley analysis[23] of the three film peaks and three substrate peaks yields the d-spacing of the (110) SrRuO$_3$ plane to be 3.908 ± 0.003 Å and the (110) DyScO$_3$ plane to be 3.943 ± 0.002 Å. This latter value is in excellent agreement with the known out-of-plane spacing of the DyScO$_3$ substrate.[24] The rocking curve for the SrRuO$_3$ 220 film peak is shown in Fig. 2(b). The peak has a full width at half maximum (FWHM) of 0.0048°, comparable to that of the underlying DyScO$_3$ substrate (FWHM = 0.0034°). Rocking curves taken along both the [001] and the $\left[\bar{1}10\right]$ orthorhombic substrate directions are shown in Fig. S4 in the supplementary material. The reciprocal space map (RSM) around the orthorhombic 240 film and substrate peaks in Fig. 2(c), shows

that the peaks are aligned in q_x and that the film is commensurately strained to the underlying substrate.

The structural quality was further investigated using scanning transmission electron microscopy (STEM). In the high-magnification STEM image shown in Fig. 2(d), the substrate-film interface is sharp and shows coherent crystallinity at both the interface and throughout the film. To get a better idea of the film quality, a larger area of the film is shown in Fig. 2(e) at a lower magnification. We do not observe any extended defects in the STEM measurements. We also find that the film is single-domain and orthorhombic by measuring x-ray diffraction ϕ-scans of the 221 orthorhombic peak as shown in Fig. S5 of the supplementary material,[25,26] and measuring RSMs for all four of the 204 pseudocubic reflections (ϕ = 0°, 90°, 180°, and 270°) as shown in Fig. S6, corresponding to the 444, 620, 44$\bar{4}$, and 260 orthorhombic reflections of the SrRuO$_3$ thin film. While our observation that SrRuO$_3$ grown on DyScO$_3$(110) is orthorhombic and untwinned (at room temperature) like prior MBE-grown SrRuO$_3$/DyScO$_3$ films,[18,27,28] as well as PLD-grown SrRuO$_3$/GdScO$_3$,[29] it differs from the tetragonal (at room temperature) SrRuO$_3$ films that have been observed when SrRuO$_3$ is grown on DyScO$_3$ by PLD.[30]

Next we characterize the film surface of this same 49.8 nm thick SrRuO$_3$ film using AFM and RHEED (see Fig. S7 in the supplementary material). The steps in the AFM image in Fig. S7(a) are far apart due to the low miscut (~0.07°) of the substrate. The emergence of small steps at the step edges on top of the larger steps indicates that the growth mechanism is most likely step-flow growth. The RHEED image along the $\left[\bar{1}10\right]$ azimuth in Fig. S7(b) shows Kikuchi lines, which indicate a flat, high quality surface during growth.

The thin films in this paper were grown utilizing a TOMBE diagram for the Sr$_{n+1}$Ru$_n$O$_{3n+1}$ Ruddlesden–Popper (RP) series, described elsewhere,[9] as a guide. By calculating the TOMBE diagram for various Ru/Sr ratios, one can qualitatively understand how higher Ru/Sr ratios shift the diagram up and to the left (see Ref. 9) and make it easier to grow phase-pure SrRuO$_3$ at higher temperatures and with fewer ruthenium vacancies. At higher temperatures, ruthenium oxides become more volatile, leading to the evaporation of oxidized ruthenium on the film surface during deposition. This increase in volatility leads to an increase in ruthenium vacancies at higher substrate temperatures. To compensate for the increased volatility, one can deposit ruthenium at a higher Ru/Sr ratio, such that there is an optimized excess amount of ruthenium flux, which yields a high quality SrRuO$_3$ film. By varying the Ru/Sr ratio and the growth temperature for different sample growths, we can achieve various levels of electrical quality in SrRuO$_3$ thin films.

We grew 11 samples of varying quality and measured the resistivity as a function of temperature. In Figs. 3(a), 3(b), and 4(a), we only display seven samples for clarity, and include all 11 samples in Fig. 4(b). Figure 3(a) shows the resistivity as a function of temperature for the seven samples. The resistivity is plotted by normalizing the resistivities to one at 300 K to illustrate the differences in the low temperature resistivity values. The RRR values of the seven samples (and all 11 samples) range from 8.83 in Sample A to 205 in Sample G. The best sample (Sample G) had a thickness of 49.8 nm; however, all of the ten other SrRuO$_3$ samples presented in this paper are of comparable thickness, ranging from 16.5 to 29.7 nm. The samples are labeled in order of increasing RRR, and the color coding
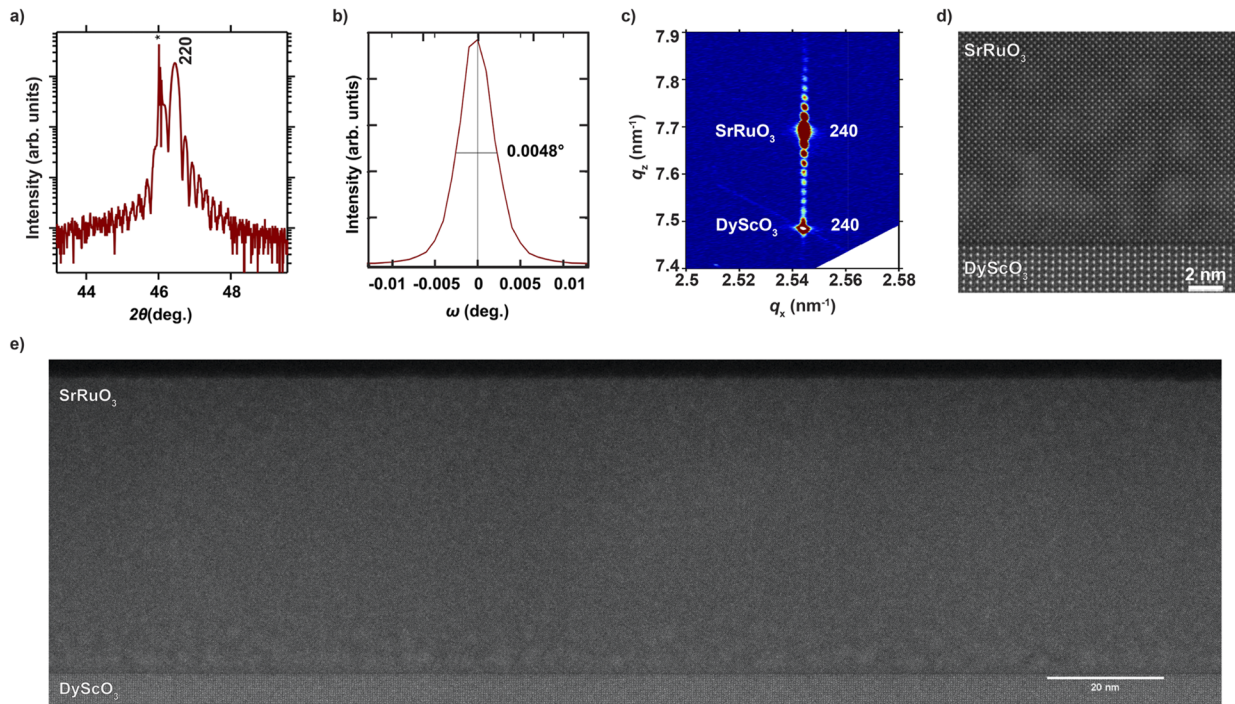
FIG. 2. Structural characterization of the high-RRR $SrRuO_3$/$DyScO_3$(110) thin film. (a) Zoom-in of the x-ray diffraction $\theta - 2\theta$ scan around the 220 orthorhombic film peak. The 220 $DyScO_3$ substrate peak is labeled with an asterisk (*). (b) Rocking curve of the orthorhombic 220 film peak. (c) Reciprocal space map of the $SrRuO_3$/$DyScO_3$(110) film showing the orthorhombic 240 peaks of both the film and substrate. (d) High-magnification STEM taken along the $[\bar{1}10]$ zone axis of the substrate. (e) Lower-magnification STEM taken along the $[\bar{1}10]$ direction to show the good quality of the film over a large area.

remains consistent in Figs. 3(a), 3(b), and 4(a). In Fig. 3(b), we show the low-temperature region of the plot from Fig. 3(a). Sample G corresponds to the sample measured in Figs. 1 and 2, and as shown in Fig. 3(b), is the lowest resistivity sample at low temperature. Nevertheless, there are two samples with only approximately double

the resistivity, corresponding to RRR values of 97.4 (Sample E) and 113.5 (Sample F). Both of these samples would also represent record-breaking RRR values for $SrRuO_3$ thin films, but unlike Sample G, these samples are still inferior to the RRR of the best $SrRuO_3$ single crystal.
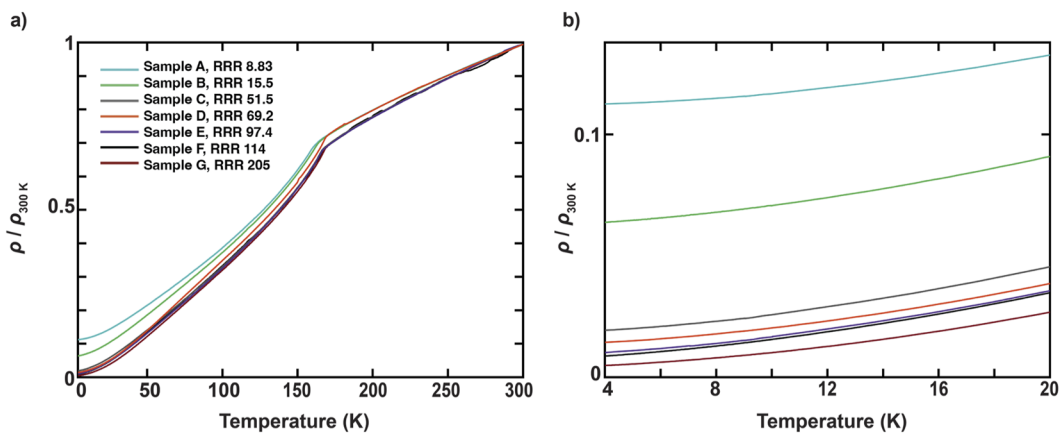
FIG. 3. Selected samples with varying RRR values ranging from 8.83 to 205. (a) Resistivities plotted as a function of temperature for seven $SrRuO_3$/$DyScO_3$(110) thin film samples with the resistivities normalized at 300 K. The samples are labeled Sample A–Sample G in order of increasing RRR. The color coding is consistent throughout the paper. (b) A zoomed-in version of (a) in the 4–20 K temperature range, illustrating the differences in the residual resistivities.
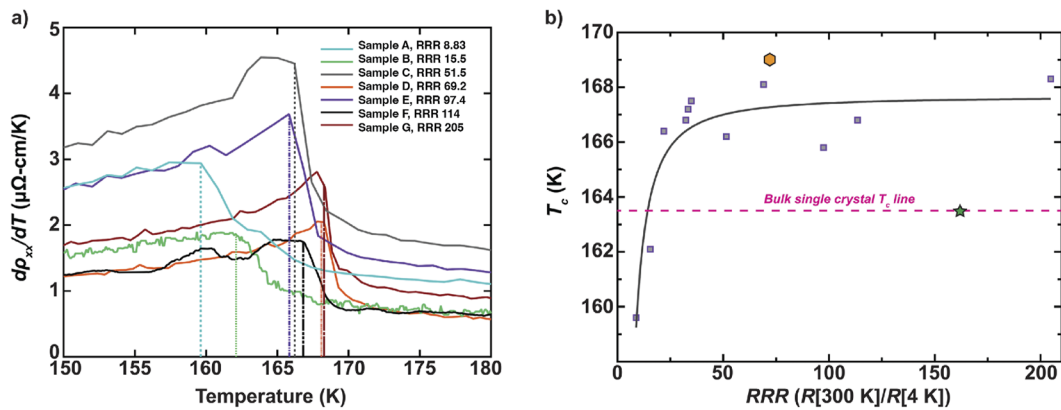
FIG. 4. (a) The derivative of the resistivity with respect to temperature for the seven SrRuO$_3$/DyScO$_3$(110) thin film samples shown in Fig. 3. (b) A plot showing T_C as a function of RRR for the seven samples in (a), along with four additional SrRuO$_3$/DyScO$_3$(110) thin film samples, for a total of 11. The green star indicates T_C for a bulk single crystal sample with an RRR (ρ [300 K]/ρ [4 K]) of 162, taken from Ref. 7. The dashed magenta line illustrates that all but two of the samples grown on DyScO$_3$(110) substrates have a higher T_C than the bulk single crystal from Ref. 7. Only Sample G has a higher RRR than the single crystal from Ref. 7. The orange hexagon indicates the RRR and T_C for the SrRuO$_3$/DyScO$_3$(110) thin film reported in Ref. 17. The solid black line is a power law fit to the data points, which acts as a guide to the eye.

SrRuO$_3$ is a widely used material, and one question that arises is whether extrinsic effects caused by defects or disorders in SrRuO$_3$ can have a significant effect on magnetic property measurements. We tackle this question by establishing the T_C of the samples in this paper (various films of different electrical quality) and comparing them based on RRR. To find the T_C, as mentioned before, we determine the derivative of the resistivity with respect to temperature and plot it as a function of temperature [see Fig. 4(a)]. The plot shows the seven samples from the previous figure. The selection of these samples is not biased based on any metric, and this becomes clear as the trend is not followed necessarily by every sample shown. Nevertheless, a general trend does emerge that higher RRR samples have a higher T_C. To highlight this trend, we plotted T_C as a function of RRR in Fig. 4(b) for all 11 samples. Figure 4(b) reveals two things: (1) Above a certain RRR threshold, T_C is mostly independent of RRR, and (2) films that are sometimes considered good quality (Sample A with an RRR of 8.83 and Sample B with an RRR of 15.5) deviate significantly in T_C from films with marginally better quality. We only realize the intrinsic T_C in SrRuO$_3$/DyScO$_3$(110) films with RRR values above ~20. Below this quality threshold, the value of T_C is depressed. This conclusion is best shown in Fig. 4(b), where the dashed magenta line represents the T_C value for the best single crystal in the literature (RRR (ρ [300 K]/ρ [4 K]) of 162).[7] The green star shows where this single crystal would belong on the RRR vs T_C plot. The orange hexagon indicates the RRR and T_C for the SrRuO$_3$/DyScO$_3$(110) thin film reported recently, for which the authors reported a record-breaking T_C of 169 K.[18]

It is important to consider systematic errors that can affect the data plotted in Fig. 4(b) and the conclusions inferred from that data. The 11 data points on our films are all measured in the same PPMS with the same mounting scheme. The observed trend substantiates that T_C does vary with the RRR of the sample. Comparisons made among SrRuO$_3$ films in the literature with high RRR could suffer from systematic errors due to the different mounting schemes and equipment used to measure SrRuO$_3$ samples in different laborato-

ries. The 6 K higher T_C exhibited by the commensurately strained and untwinned SrRuO$_3$/DyScO$_3$(110) with the highest RRR compared with the SrRuO$_3$ single crystal with the highest RRR would appear to be sufficiently different to imply that strain can enhance the T_C of SrRuO$_3$. On the other hand, the 0.7 K higher T_C of the high RRR SrRuO$_3$/DyScO$_3$(110) in Ref. 18 compared to the high RRR SrRuO$_3$/DyScO$_3$(110) of this study could be due to a systematic difference between resistivity measurement systems.

Variations in thickness and growth conditions can affect the RRR of the SrRuO$_3$ thin films. In Figs. S8–S11, we plot the RRR of all 11 samples as a function of thickness, growth rate, substrate temperature, and ruthenium-to-strontium ratio, respectively. As shown in Fig. S8, there is a correlation between the RRR and film thickness, although weak. Thicker films tend to have a higher RRR because, in thicker films, the interface is a smaller percentage of the film volume. While thickness shows a weak linear relationship to RRR, the other three parameters (growth rate, substrate temperature, and ruthenium-to-strontium ratio) are not linearly related to RRR. It is important to note that all three of these variables are dependent on each other. For example, a higher ruthenium-to-strontium ratio is necessary at higher growth temperatures as the volatility of RuO$_x$ (with RuO$_3$ being the most volatile) increases with substrate temperature.[9] In addition, the growth rate is set by the strontium flux, which is the denominator of the ruthenium-to-strontium ratio. Since each of the samples has a different growth rate, substrate temperature, and ruthenium-to-strontium ratio, the trends are not clear in Figs. S9–S11. Nonetheless, in Figs. S10 and S11, there appears to be a peak in the RRR for films grown at a substrate temperature around 660–665 °C and a ruthenium-to-strontium ratio of about 2. There are likely multiple Goldilocks regions of substrate temperature and ruthenium-to-strontium ratio yielding films with high RRR; these could be outlined in future studies.

If we assume that the properties exhibited by Sample G with an RRR of 205 are nearly intrinsic, then we can conclude that the intrinsic T_C of SrRuO$_3$ commensurately strained to DyScO$_3$(110) is near

168.3 K plus/minus some error bar reflecting the systematic error in the absolute temperature of the film compared to the temperature measured by our PPMS. There is a distinct threshold between the samples with RRRs of 15.5 and 22.0, as shown in Fig. 4(b). Somewhere in that RRR range is the threshold, above which the electrical quality of the film has minimal effect on T_C and below which there is a large effect on T_C. In fact, the T_C of the SrRuO$_3$ films seems to saturate for a large range of RRRs (22–205) above this threshold, further indicating that this is the intrinsic T_C with some amount of error. Others have discovered similar relationships in SrRuO$_3$ thin films recently.[14] The threshold identified here, roughly 20, is important because below the threshold, the enhanced T_C is not observed, meaning that the intrinsic properties cannot be measured with such samples.

IV. CONCLUSION

To summarize, we have grown an untwinned, single-domain SrRuO$_3$/DyScO$_3$(110) thin film with a RRR of 205, which represents a new RRR record for both films and bulk single crystals. We have measured the T_C of this high-quality thin film to be 168.3 K. In comparing the T_C of various high RRR samples grown on DyScO$_3$(110) with the best bulk single crystal, we find that the epitaxial strain provided by the DyScO$_3$(110) substrate enhances T_C in SrRuO$_3$ with respect to a bulk value of 163.5 K. Therefore, when measuring T_C, and likely other magnetic properties of SrRuO$_3$, it is imperative that the RRR of the thin films studied exceed ~20. Understanding the intrinsic properties and identifying the minimum viable electrical quality is important for future studies, and we hope this work leads to the discovery of new intrinsic properties in SrRuO$_3$ and SrRuO$_3$-based heterostructures.

SUPPLEMENTARY MATERIAL

Additional data and characterization relevant to this article and referenced in the main text—including Figs. S1–S11—are provided in the supplementary material.

ACKNOWLEDGMENTS

AUTHOR DECLARATIONS

Conflict of Interest

The authors have no conflicts to disclose.

Author Contributions

Nathaniel J. Schreiber: Conceptualization (equal); Formal analysis (equal); Investigation (equal); Writing – original draft (equal); Writing – review & editing (equal). **Ludi Miao**: Investigation (supporting); Methodology (supporting); Writing – original draft (supporting); Writing – review & editing (supporting). **Hari P. Nair**: Investigation (supporting); Methodology (supporting); Writing – review & editing (supporting). **Jacob P. Ruf**: Investigation (supporting); Methodology (supporting); Writing – review & editing (supporting). **Lopa Bhatt**: Formal analysis (supporting); Investigation (supporting); Methodology (supporting); Writing – original draft (supporting); Writing – review & editing (supporting). **Yorick A. Birkholzer**: Investigation (supporting); Methodology (supporting); Writing – original draft (supporting); Writing – review & editing (supporting). **George N. Kotsonis**: Investigation (supporting); Methodology (supporting); Writing – original draft (supporting); Writing – review & editing (supporting). **Lena F. Kourkoutis**: Funding acquisition (supporting); Supervision (supporting); Writing – review & editing (supporting). **Kyle M. Shen**: Funding acquisition (supporting); Supervision (supporting); Writing – review & editing (supporting). **Darrell G. Schlom**: Funding acquisition (lead); Supervision (lead); Writing – original draft (supporting); Writing – review & editing (equal).

DATA AVAILABILITY

The data that support the findings of this study are available within the article and its supplementary material and from the corresponding author upon reasonable request.

REFERENCES

[1] Y. Maeno, H. Hashimoto, K. Yoshida, S. Nishizaki, T. Fujita, J. G. Bednorz, and F. Lichtenberg, Nature **372**, 532 (1994).

[2] J. P. Ruf, H. Paik, N. J. Schreiber, H. P. Nair, L. Miao, J. K. Kawasaki, J. N. Nelson, B. D. Faeth, Y. Lee, B. H. Goodge, B. Pamuk, C. J. Fennie, L. F. Kourkoutis, D. G. Schlom, and K. M. Shen, Nat. Commun. **12**, 59 (2021).

[3] J. M. Longo, P. M. Raccah, and J. B. Goodenough, J. Appl. Phys. **39**, 1327 (1968).

[4] F. Nakamura, M. Sakaki, Y. Yamanaka, S. Tamaru, T. Suzuki, and Y. Maeno, Sci. Rep. **3**, 2536 (2013).

[5] A. Bose, N. J. Schreiber, R. Jain, D.-F. Shao, H. P. Nair, J. Sun, X. S. Zhang, D. A. Muller, E. Y. Tsymbal, D. G. Schlom, and D. C. Ralph, Nat. Electron. **5**, 267 (2022).

[6] A. P. Mackenzie, R. K. W. Haselwimmer, A. W. Tyler, G. G. Lonzarich, Y. Mori, S. Nishizaki, and Y. Maeno, Phys. Rev. Lett. **80**, 161 (1998).

[7] N. Kikugawa, R. Baumbach, J. S. Brooks, T. Terashima, S. Uji, and Y. Maeno, Cryst. Growth Des. **15**, 5573 (2015).

[8] M. Izumi, K. Nakazawa, Y. Bando, Y. Yoneda, and H. Terauchi, J. Phys. Soc. Jpn. **66**, 3893 (1997).

[9] H. P. Nair, Y. Liu, J. P. Ruf, N. J. Schreiber, S.-L. Shang, D. J. Baek, B. H. Goodge, L. F. Kourkoutis, Z.-K. Liu, K. M. Shen, and D. G. Schlom, APL Mater. **6**, 046101 (2018).

[10]K. Takiguchi, Y. K. Wakabayashi, H. Irie, Y. Krockenberger, T. Otsuka, H. Sawada, S. A. Nikolaev, H. Das, M. Tanaka, Y. Taniyasu, and H. Yamamoto, Nat. Commun. **11**, 1090 (2020).

[11]Y. K. Wakabayashi, M. Kobayashi, Y. Takeda, K. Takiguchi, H. Irie, S.-i. Fujimori, T. Takeda, R. Okano, Y. Krockenberger, Y. Taniyasu, and H. Yamamoto, Phys. Rev. Mater. **5**, 124403 (2021).

[12]D. Kan, R. Aso, H. Kurata, and Y. Shimakawa, J. Appl. Phys. **113**, 173912 (2013).

[13]Q. Gan, R. A. Rao, C. B. Eom, J. L. Garrett, and M. Lee, Appl. Phys. Lett. **72**, 978 (1998).

[14]Y. K. Wakabayashi, S. Kaneta-Takada, Y. Krockenberger, K. Takiguchi, S. Ohya, M. Tanaka, Y. Taniyasu, and H. Yamamoto, AIP Adv. **11**, 035226 (2021).

[15]B. Dabrowski, O. Chmaissem, P. W. Klamut, S. Kolesnik, M. Maxwell, J. Mais, Y. Ito, B. D. Armstrong, J. D. Jorgensen, and S. Short, Phys. Rev. B **70**, 014423 (2004).

[16]G. Kim, K. Son, Y. E. Suyolcu, L. Miao, N. J. Schreiber, H. P. Nair, D. Putzky, M. Minola, G. Christiani, P. A. van Aken, K. M. Shen, D. G. Schlom, G. Logvenov, and B. Keimer, Phys. Rev. Mater. **4**, 104410 (2020).

[17]Y. K. Wakabayashi, T. Otsuka, Y. Krockenberger, H. Sawada, Y. Taniyasu, and H. Yamamoto, APL Mater. **7**, 101114 (2019).

[18]Y. K. Wakabayashi, S. Kaneta-Takada, Y. Krockenberger, Y. Taniyasu, and H. Yamamoto, ACS Appl. Electron. Mater. **3**, 2712 (2021).

[19]A. P. MacKenzie, J. W. Reiner, A. W. Tyler, L. M. Galvin, S. R. Julian, M. R. Beasley, T. H. Geballe, and A. Kapitulnik, Phys. Rev. B **58**, R13318 (1998).

[20]L. J. van der Pauw, Philips Res. Rep. **20**, 220 (1958).

[21]Y. Wang, G. Bossé, H. P. Nair, N. J. Schreiber, J. P. Ruf, B. Cheng, C. Adamo, D. E. Shai, Y. Lubashevsky, D. G. Schlom, K. M. Shen, and N. P. Armitage, Phys. Rev. Lett. **125**, 217401 (2020).

[22]S. A. Stepanov, Proc. SPIE **5536**, 16 (2004).

[23]J. B. Nelson and D. P. Riley, Proc. Phys. Soc. **57**, 160 (1945).

[24]R. Uecker, B. Velickov, D. Klimm, R. Bertram, M. Bernhagen, M. Rabe, M. Albrecht, R. Fornari, and D. G. Schlom, J. Cryst. Growth **310**, 2649 (2008).

[25]C. B. Eom, R. J. Cava, R. M. Fleming, J. M. Phillips, R. B. van Dover, J. H. Marshall, J. W. P. Hsu, J. J. Krajewski, and W. F. Peck, Jr., Science **258**, 1766 (1992).

[26]J.-P. Maria, S. Trolier-McKinstry, D. G. Schlom, M. E. Hawley, and G. W. Brown, J. Appl. Phys. **83**, 4373 (1998).

[27]J. R. Contreras, Ph.D. thesis, Universität zu Köln, 2003.

[28]Y.-H. Chu, Q. Zhan, L. W. Martin, M. P. Cruz, P.-L. Yang, G. W. Pabst, F. Zavaliche, S.-Y. Yang, J.-X. Zhang, L.-Q. Chen, D. G. Schlom, I.-N. Lin, T.-B. Wu, and R. Ramesh, Adv. Mater. **18**, 2307 (2006).

[29]D. Kan, R. Aso, H. Kurata, and Y. Shimakawa, Adv. Funct. Mater. **23**, 1129 (2013).

[30]K. J. Choi, S. H. Baek, H. W. Jang, L. J. Belenky, M. Lyubchenko, and C.-B. Eom, Adv. Mater. **22**, 759 (2010).
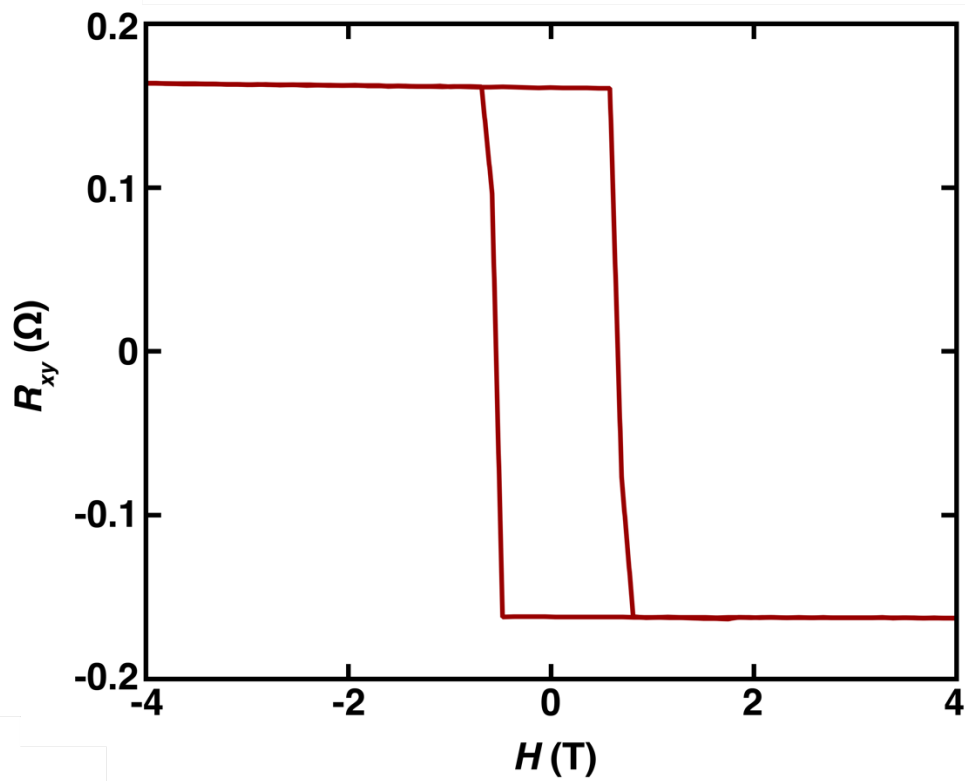
**FIG. S1.** Hall measurement of the high-RRR SrRuO₃/DyScO₃(110) thin film at a temperature of 100 K. The sample is measured with the magnetic field aligned along the magnetic easy axis (~50° away from the surface normal vector).
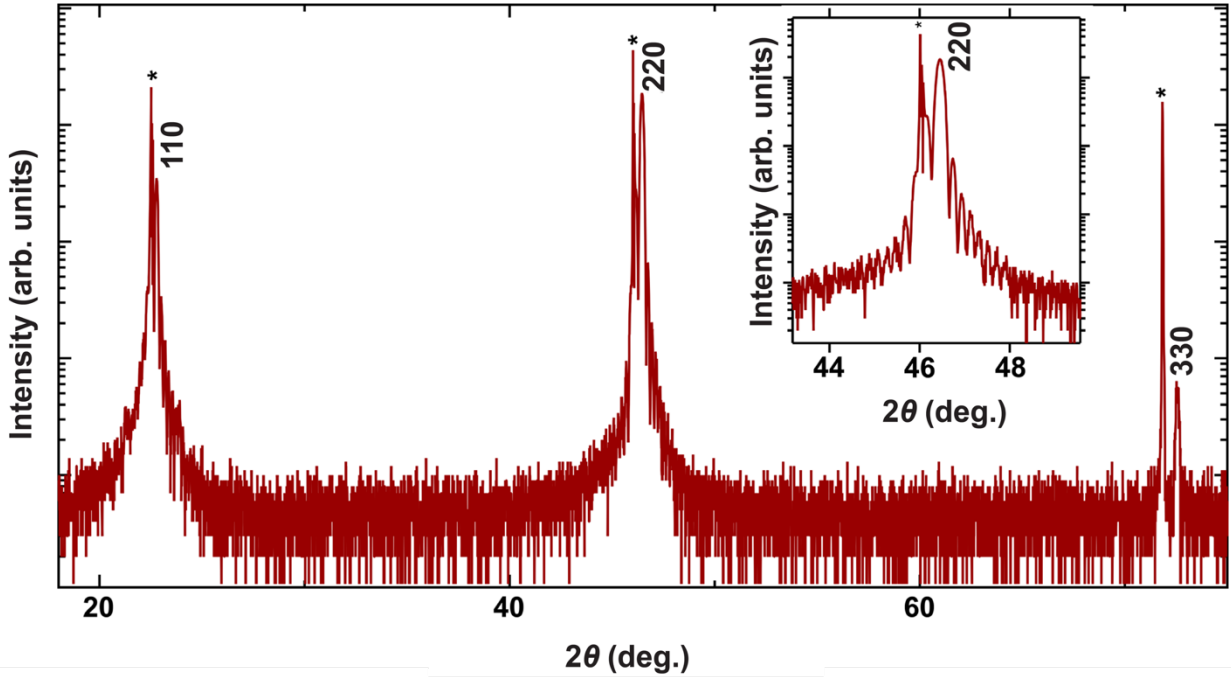
FIG. S2. X-ray diffraction $\theta - 2\theta$ scan of the high-RRR SrRuO$_3$/DyScO$_3$(110) thin film. The inset is the zoom-in from the Fig. 1(a). The SrRuO$_3$ film peaks are labeled with orthorhombic indices. The DyScO$_3$ substrate peaks are labeled with an asterisk (*).
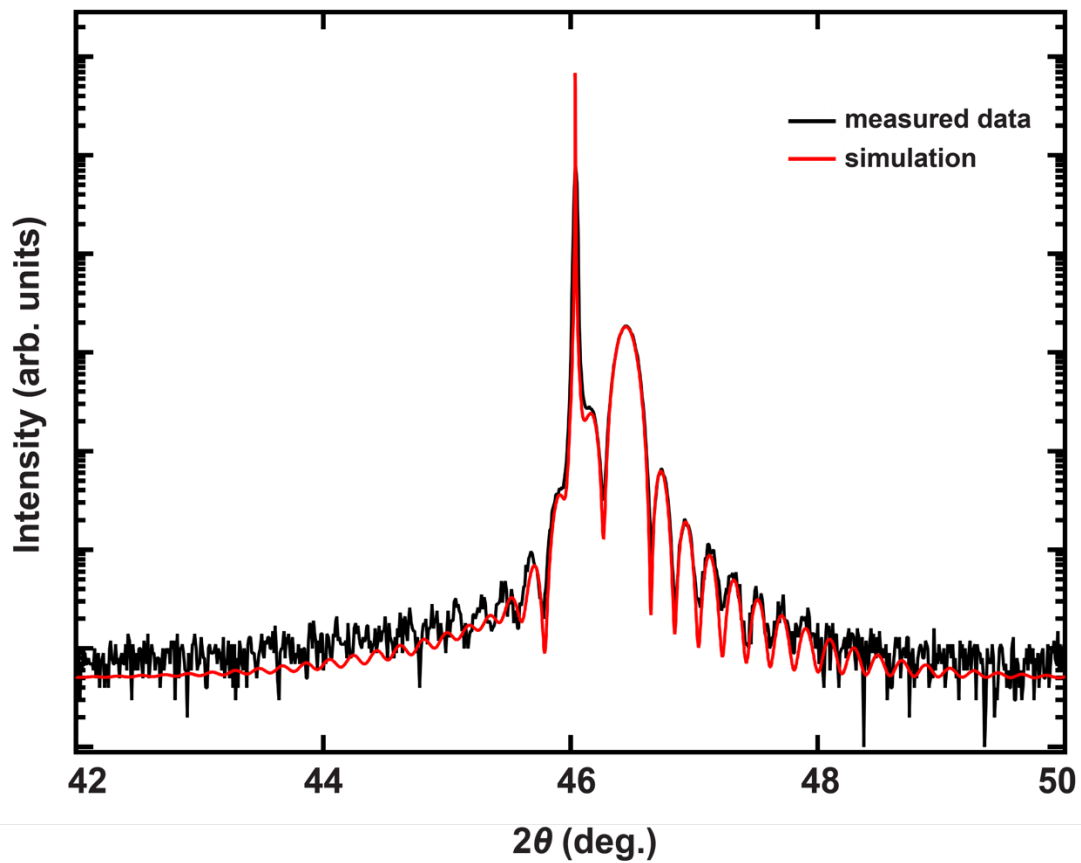
Fig. S3. Shown are the XRD data around the 220 orthorhombic film peak from Fig. S1 and the dynamical X-ray diffraction simulation[22] of the region plotted together. From this simulation, we find that the thickness of the high-RRR SrRuO₃ sample is 49.8 ± 1 nm.
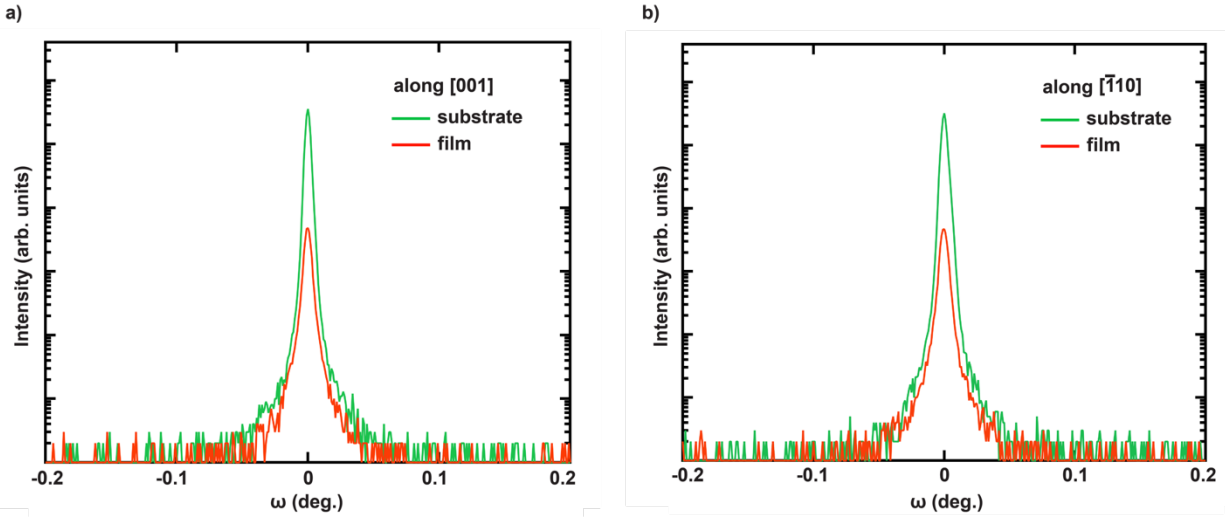
FIG. S4. Rocking curves of the 220 orthorhombic film peak taken with the beam **(a)** parallel to the substrate [001] direction and **(b)** parallel to the substrate $[\bar{1}10]$ direction.
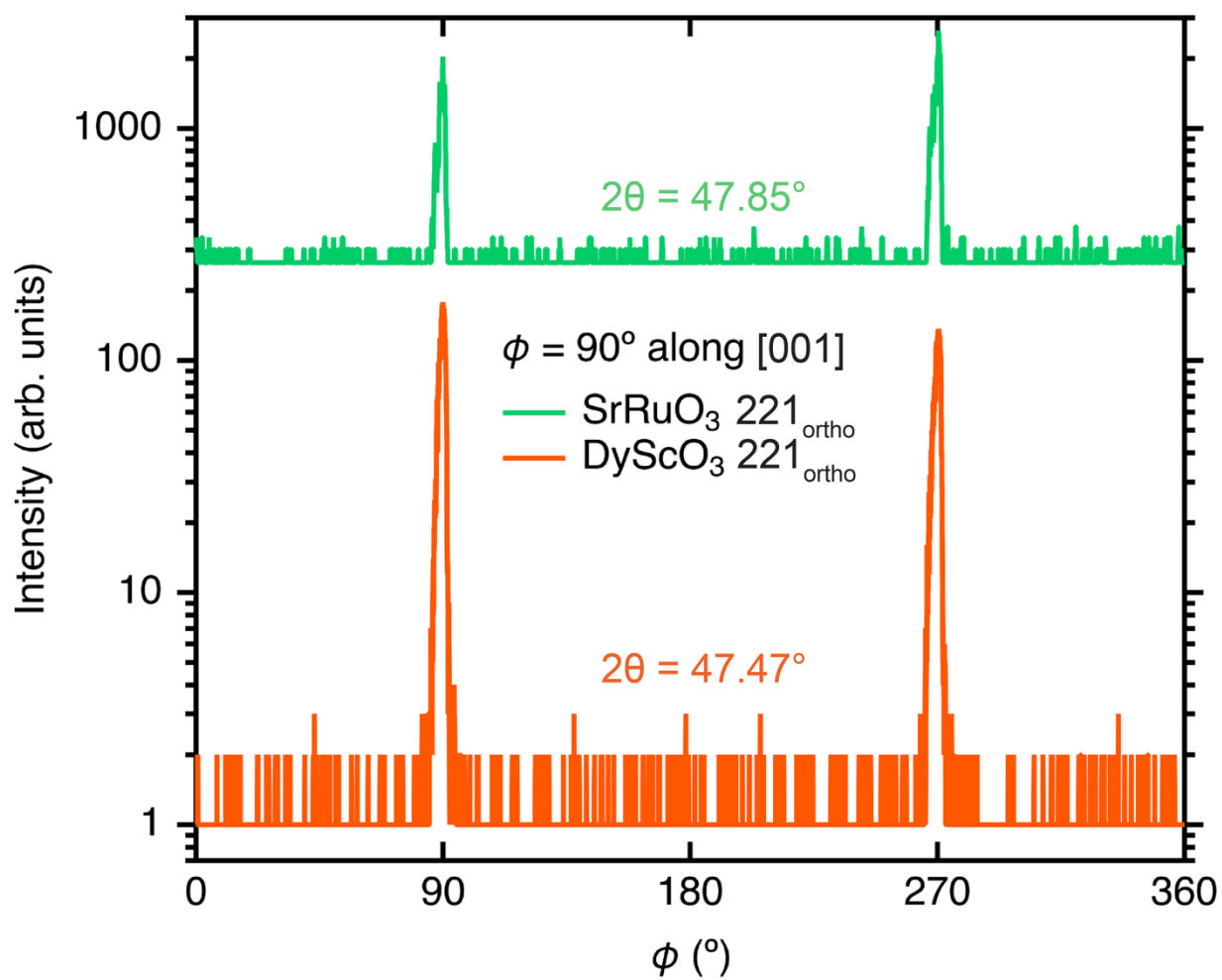
FIG. S5. ϕ-scans of the 221 orthorhombic peaks, showing two peaks, indicating the film is made up of one domain.
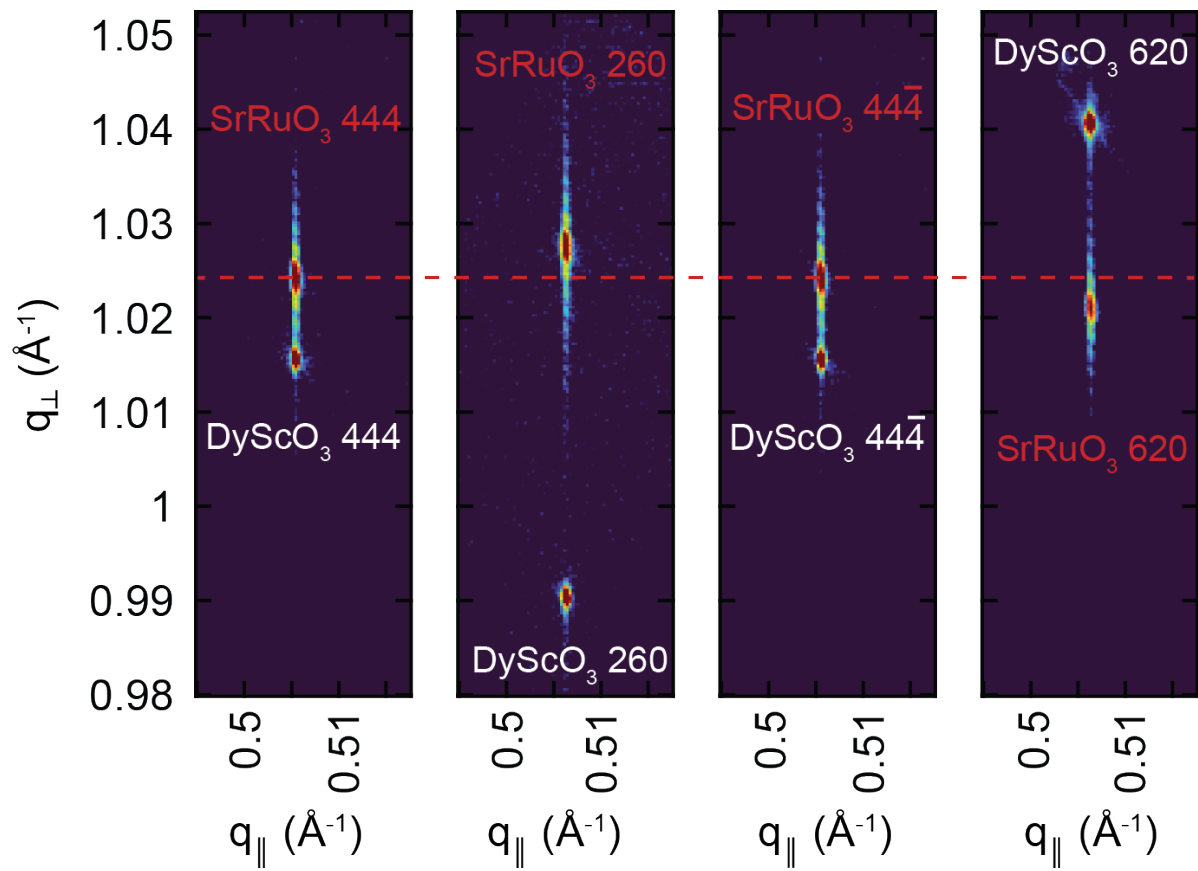
Fig. S6. Reciprocal space maps showing all four of the 204 pseudocubic SrRuO$_3$ reflections (ϕ = 0°, 90°, 180°, and 270°), corresponding to the 444, 620, 44$\bar{4}$, and 260 orthorhombic reflections of SrRuO$_3$.
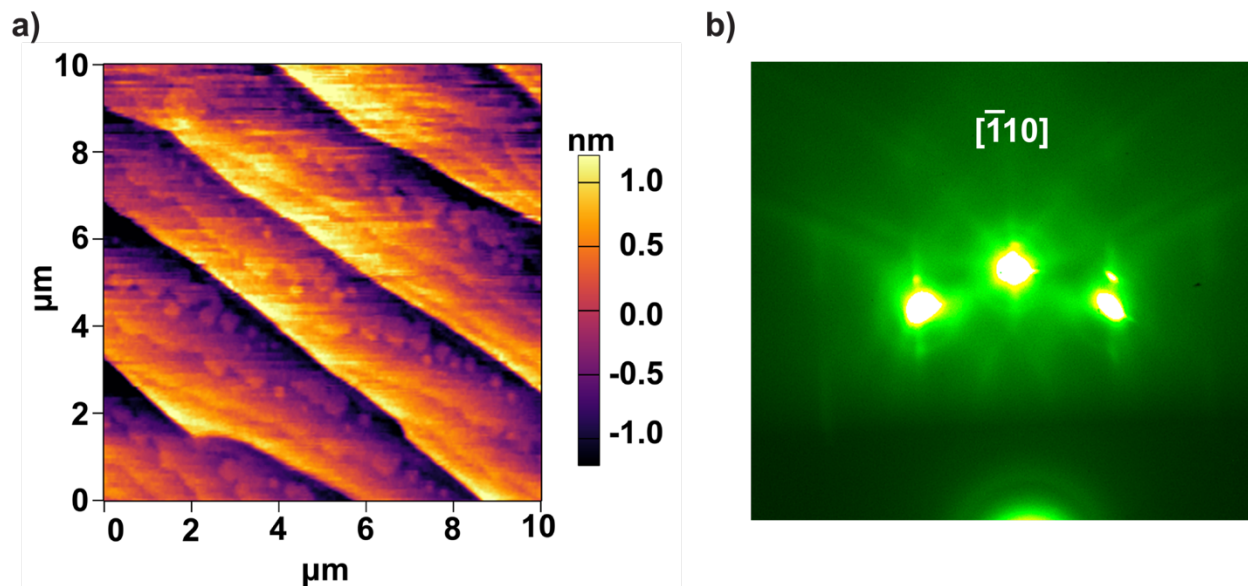
FIG. S7. Surface Characterization of the 49.8 nm thick film with RRR=205. **(a)** Atomic force microscopy image showing a 10 μm x 10 μm area on the surface of the film. **(b)** RHEED image taken along the $[\bar{1}10]$ orthorhombic azimuth immediately following growth of the 49.8 nm thick film. The image was taken at growth temperature.

In **Figs. S8**, **S9**, **S10**, and **S11** circular data points represent the 7 samples shown in **Figs. 3** and **4(a)** (Samples A-G), and have the same coloring scheme as the aforementioned figures in the main text. The remaining 4 samples are represented by different shapes (diamond, square, triangle, and x) for tracking across growth conditions.
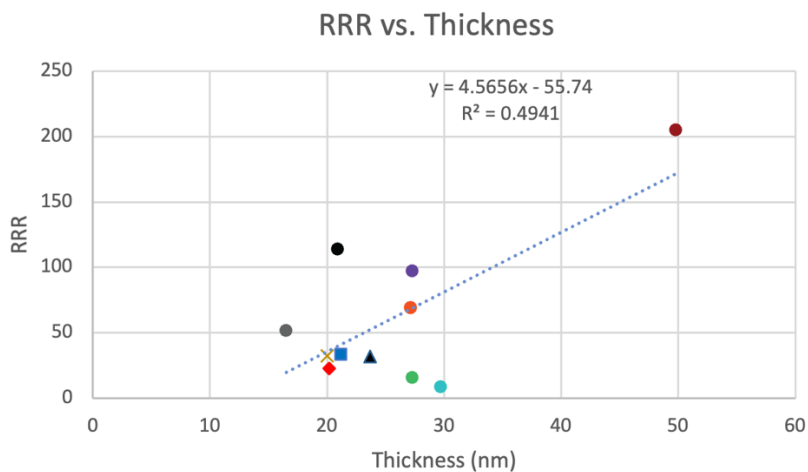
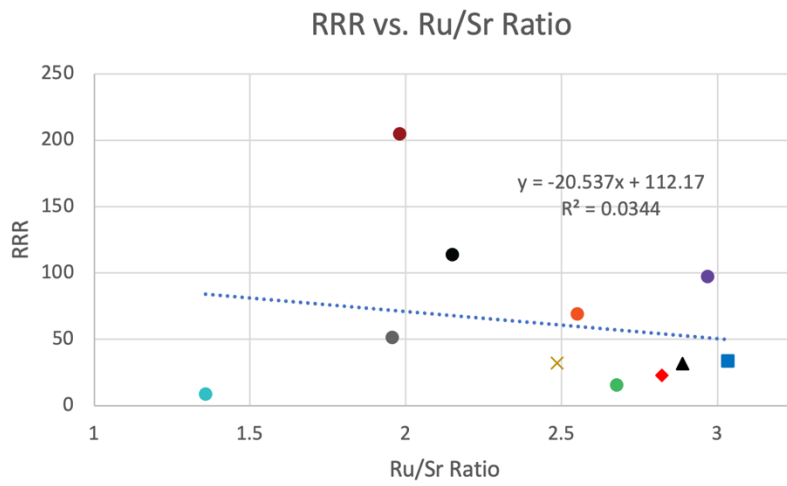**FIG. S8.** RRR plotted as a function of thickness for the 11 samples.
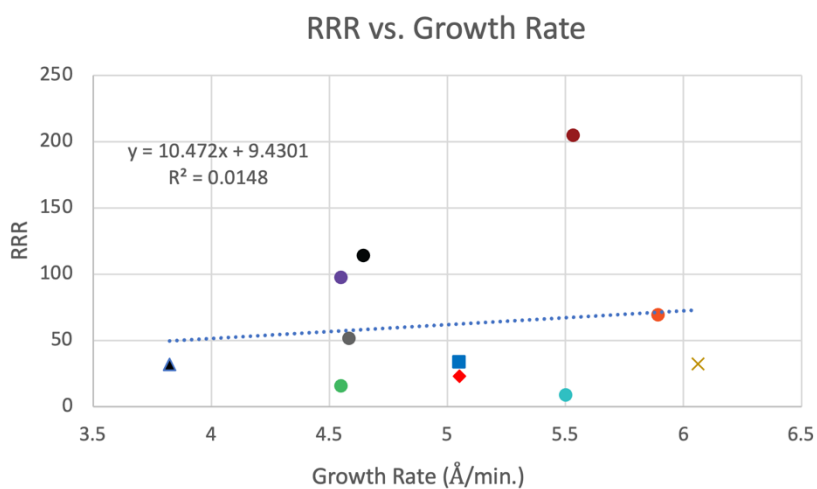
FIG. S9. RRR plotted as a function of growth rate for the 11 samples.
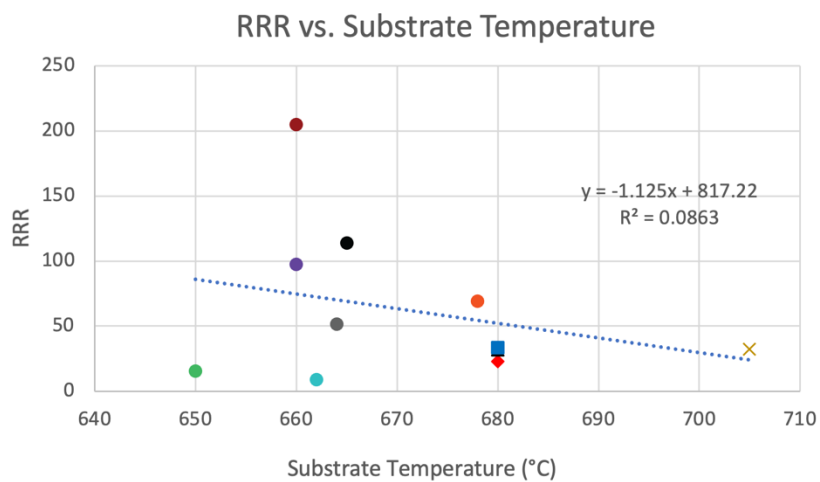
FIG. S10. RRR plotted as a function of substrate temperature for the 11 samples.

FIG. S11. RRR plotted as a function of ruthenium-to-strontium ratio (Ru/Sr) for the 11 samples.